Dressed-state analysis of efficient three-dimensional atom localization in a ladder-type three-level atomic system

2016 Laser Phys. 26 075203

(http://iopscience.iop.org/1555-6611/26/7/075203)

IOP Publishing | Astro Ltd Laser Physics
Laser Phys. **26** (2016) 075203 (7pp) doi:10.1088/1054-660X/26/7/075203

Dressed-state analysis of efficient three-dimensional atom localization in a ladder-type three-level atomic system

Zhonghu Zhu[1], Wen-Xing Yang[1], Ai-Xi Chen[2], Shaopeng Liu[1] and Ray-Kuang Lee[3]

[1] Department of Physics, Southeast University, Nanjing 210096, People's Republic of China
[2] Department of Applied Physics, East China Jiaotong University, Nanchang 330013, People's Republic of China
[3] Institute of Photonics Technologies, National Tsing-Hua University, Hsinchu 300, Taiwan, Republic of China

E-mail: wenxingyang2@126.com

Received 18 April 2016, revised 24 May 2016
Accepted for publication 24 May 2016
Published 22 June 2016

Abstract

We study the control of high-precision three-dimensional (3D) atom localization by measuring the population of the excited state in a ladder-type three-level atomic system driven by a weak probe field and a control field, together with three mutually perpendicular standing-wave fields. We find that the precision of 3D atom localization in volumes depends sensitively on the frequency detuning of the probe field and the intensity of the control field. Most importantly, we show that adjusting the phase shifts associated with the standing-wave fields leads to a redistribution of the atoms and a significant change of the atomic coherence, so that the atom can be localized in volumes that are substantially smaller than a cubic optical wavelength.

Keywords: three-dimensional atom localization, quantum interference, the standing-wave field

(Some figures may appear in colour only in the online journal)

1. Introduction

During the past few decades, the spatial localization of an atom based on position-dependent atom-field interaction has been extensively studied in the field of the precision position measurement of atoms via different optical techniques [1–4]. Based on atomic coherence and quantum interference effects [5–9], earlier schemes for atom localization in various atomic configurations mainly involve one-dimensional (1D) atom localization and two-dimensional (2D) atom localization. For 1D atom localization, several proposals for improving the accuracy of measurements have been made via different measurement schemes, such as the measurement of resonance fluorescence [10, 11], spatially dependent spontaneous emission [12–14] and probe absorption spectra [15, 16], coherent population trapping (CPT) [17], dark resonances [18], and multiple simultaneous measurements [19–21]. In these schemes, standing-wave driving fields have been used to encode position information into the intensity pattern via the position-dependent Rabi frequency. Compared with 1D atom localization, 2D atom localization has a better prospect of application, and has hence been extensively studied in recent years. By interacting with two orthogonal standing-wave fields, the measurements of the upper-level population [22], the controlled spontaneous emission [23] and double-dark resonances [24] are applied to achieve 2D atom localization. Afterwards, several schemes for achieving high-precision and high-resolution 2D atom localization have been put forward [25–32] in differently configured atomic systems. It is worth noting that for high-precision 2D atom localization, one can obtain mere subwavelength localization as well as the spatial structuring of the atomic locations, and the maximum probability of finding the atom at an expected position in one period of the standing-wave fields can reach 100%.

More recently, much attention has been paid to three-dimensional (3D) atom localization based on the interaction of the atoms with three mutually perpendicular standing-wave fields. Possible applications of 3D atom localization

may include high-precision position-dependent state selective chemical reactions. By applying three mutually perpendicular standing-wave fields, Qi and co-workers [33] have presented a scheme for 3D atom localization based on electromagnetically induced transparency (EIT) by measuring the probe absorption in a five-level M-type atomic system. Ivanov and co-workers [34] have obtained different 3D periodic structures in 3D space via the measurement of the atomic-level population in a four-level tripod-type atomic system. In addition, phase-sensitive 3D atom localization has been achieved in [35] by measuring the absorption spectra. However, these proposals have not provided a promising way of achieving high-precision and high-resolution 3D atom localization.

To further improve the precision of 3D atom localization, we propose a scheme for realizing a high-precision method by measuring the population of the excited state in a ladder-type three-level atomic system. Although such atomic models have been used to realize 3D atom localization [36], we have provided a new way of achieving high-precision localization, and our proposal has more advantages over [36]. The major differences are obtained as follows. First, our scheme is based on the measurement of the upper-level population via the interaction of the atoms with two laser fields as well as three mutually perpendicular standing-wave fields. However, the scheme of [36] is based on the measurement of spontaneous emission, which is difficult to carry out in practical experiments. The reason for this is that spontaneous emission is a random process, and the frequency of the spontaneously emitted photon is hard to control. Moreover, it is impossible to measure the spontaneous emission spectrum in [36] due to the absence of the condition of spontaneous emission. Second, the atom can be completely localized in one subspace by adjusting the phase shifts of three perpendicular standing-wave fields with slightly different wavelengths, and the maximum probability of finding the atom in 3D space is increased by a factor of eight compared with the previous schemes [33, 34]. That is to say, we have obtained a new way of achieving high-precision 3D atom localization. However, such similar proposals have not been used in [36]. Third, we have discussed how the excited population modifies the 3D atom localization behavior, and one finds that the precision of 3D atom localization almost remains unchanged as the value of the excited population increases. That is to say, in our present scheme, high-precision 3D atom localization can be achieved in a wide range of excited state population distribution. However, [36] has not discussed such results. Therefore, our scheme has more advantages than other schemes [33–36] for 3D atom localization.

2. Theoretical model and basic equations

Let us consider a ladder-type three-level atomic system with a lower state $|1\rangle$ and two excited states $|2\rangle$ and $|3\rangle$ as shown in figure 1(a). The transition between levels $|1\rangle$ and $|2\rangle$ (with transition frequency ω_{21}) is coupled by a weak probe field $E_{\rm p}$ (with angular frequency ω_p and a Rabi frequency $2\,\Omega_{\rm p}$). The relevant standing-wave field (with position-dependent Rabi frequency $G_s(x, y, z)$) and an extra control field $E_{\rm c}$ (with a Rabi

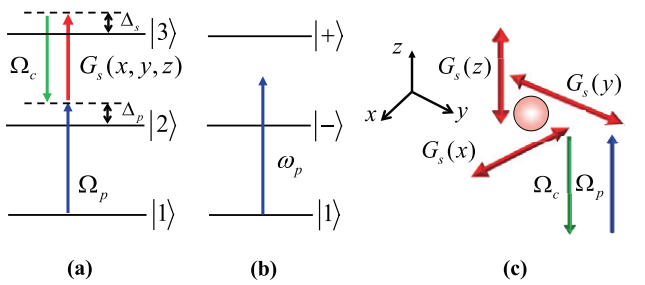

Figure 1. (a) The energy-level diagram of a ladder-type three-level atomic system interacting with a weak probe field $\Omega_{\rm p}$, a coherent coupling field $\Omega_{\rm c}$ and a combination of three mutually perpendicular standing-wave fields $G_{\rm s}(x, y, z)$, where $G_{\rm s}(x, y, z)$ corresponds to the combination of three orthogonal standing-wave fields. $\Delta_{\rm p}$ represents the single-photon detuning. $\Delta_{\rm s}$ stands for two-photon detuning. (b) A schematic of the dressed-state picture. In the presence of the control field $\Omega_{\rm c}$ and the combination of three mutually perpendicular standing-wave fields $G_{\rm s}(x, y, z)$, the corresponding transition $|2\rangle \longleftrightarrow G_{\rm s}(x, y, z) + \Omega_{\rm c}|3\rangle$ gives rise to the two dressed states $|+\rangle$ and $|-\rangle$. (c) Three orthogonal standing-wave fields $G_{\rm s}(x)$, $G_{\rm s}(y)$ and $G_{\rm s}(z)$ aligning along the x, y and z directions form a 3D space, while the probe field $\Omega_{\rm p}$ and the coherent coupling field $\Omega_{\rm c}$ propagate along the z direction.

frequency $2\,\Omega_{\rm c}$) simultaneously couple the transition between levels $|2\rangle$ and $|3\rangle$ (with transition frequency ω_{32}). It is worth pointing out that $G_s(x, y, z)$ corresponds to the combination of three orthogonal standing-wave fields that drive the transition between levels $|2\rangle$ and $|3\rangle$, i.e.

$$G_s(x, y, z) = G_{\rm s}(x) + G_{\rm s}(y) + G_{\rm s}(z), \tag{1}$$

where $G_{\rm s}(x)$, $G_{\rm s}(y)$ and $G_{\rm s}(z)$ are also the combinations of two orthogonal standing-wave fields aligning along the corresponding x, y and z directions, respectively (see figure 1(c)), i.e.

$$G_{\rm s}(x) = \Omega_1\left[\sin(\kappa_1 x + \varphi) + \sin(\kappa_2 x)\right], \tag{2}$$

$$G_{\rm s}(y) = \Omega_2\left[\sin(\kappa_3 y + \phi) + \sin(\kappa_4 y)\right], \tag{3}$$

$$G_{\rm s}(z) = \Omega_3\left[\sin(\kappa_5 z + \eta) + \sin(\kappa_6 z)\right], \tag{4}$$

with $\kappa_i = 2\pi/2\pi\lambda_i\lambda_i$ $(i = 1 - 6)$ being the wave vectors corresponding to the wavelength λ_i of the relevant standing-wave fields. The parameters φ, ϕ and η are the phase shifts of the relevant standing-wave fields corresponding to wave vectors κ_1, κ_3 and κ_5, respectively. An atom moves along the z direction and passes through the intersecting region of the three mutually perpendicular standing-wave fields in the 3D space. As a result, the interaction between the atom and the standing-wave fields is spatially dependent on the 3D space.

Here we assume that the center-of-mass position distribution of the atom along the directions of the standing-wave fields is nearly constant and we can ignore the kinetic energy of the atom in the Hamiltonian by applying the Raman–Nath approximation [37]. By choosing $H_0 = \omega_p|2\rangle\langle 2| + (\omega_p + \omega_s)|3\rangle\langle 3|$ and taking level $|1\rangle$ as the energy origin, under the electric dipole approximation (EDA) and the rotating-wave approximation (RWA), the interaction Hamiltonian of the present atomic system is given by ($\hbar = 1$):

$$H_{\rm int} = -\Delta_{\rm p}|2\rangle\langle 2| - \Delta_{\rm s}|3\rangle\langle 3| - [\Omega_{\rm p}|2\rangle\langle 1| + (G_{\rm s}(x,y,z) + \Omega_{\rm c})|3\rangle\langle 2| + {\rm H.c.}], \quad (5)$$

where the symbol H.c. represents the Hermitian conjugation, and $\omega_c = \omega_s$. $\Delta_{\rm p} = \omega_p - \omega_{21}$ represents the single-photon detuning. $\Delta_{\rm s} = \omega_p + \omega_s - \omega_{31}$ stands for the two-photon detuning. $\Omega_{\rm p} = \frac{\mu_{21}E_{\rm p}}{2\hbar}$ and $\Omega_{\rm c} = \frac{\mu_{32}E_{\rm c}}{2\hbar}$ are the half Rabi frequencies of the laser fields for the relevant driven transitions, where $\mu_{ij} = \vec{\mu}_{ij}\cdot\vec{e}_{\rm L}$ $(i, j = 1-3)$ denotes the dipole matrix moment for the relevant optical transition from level $|i\rangle$ to level $|j\rangle$ with $\vec{e}_{\rm L}$ denoting the unit polarization vector of the corresponding laser field. In the following calculations, for simplicity, we assume $\Omega_1 = \Omega_2 = \Omega_3 = \Omega_{\rm s}$ and set $\Omega_{\rm p}$, $\Omega_{\rm c}$ and $\Omega_{\rm s}$ as real parameters.

The dynamics of this system can be described by using the probability amplitude equations. Then the wave function of the present atomic system at time t can be expressed in terms of the state vectors as

$$|\psi(t)\rangle = \int {\rm d}x{\rm d}y{\rm d}z f(x,y,z)|x,y,z\rangle [A_1(x,y,z;t)|1\rangle + A_2(x,y,z;t)|2\rangle + A_3(x,y,z;t)|3\rangle], \quad (6)$$

where $A_i(x, y, z;t)$ $(i = 1-3)$ denotes the time- and position-dependent probability amplitude for the atom in level $|i\rangle$, and $f(x, y, z)$ is the centre-of-mass wave function of the atom.

Hence, the conditional spatial-position-dependent probability distribution of the atoms can be given by

$$P(x,y,z;t|2) = |\mathcal{N}|^2 |f(x,y,z)|^2 |A_2(x,y,z;t)|^2, \quad (7)$$

where $\mathcal{N}$ is a normalization factor. Here, we assume that the center-of-mass wave function of the atom $f(x, y, z)$ is nearly constant over many wavelengths of the standing-wave fields in the (x, y, z) space, which remains unchanged even after interaction with the optical fields. That is to say, the conditional position probability distribution $P(x, y, z; t|2)$ is mainly determined by the term $|A_2(x, y, z; t)|^2$. Therefore, the measurement of the population in level $|2\rangle$ can directly obtain the position information of the atom when the atom passes through the standing-wave fields.

By substituting the interaction Hamiltonian given by equation (5) and the atomic wave function given by equation (6) into the time-dependent Schrödinger wave equation $\mathrm{i}\frac{\partial|\psi(t)\rangle}{\partial t} = H_{\rm int}|\psi(t)\rangle$, the coupled equations of motion for the time evolution of the atomic probability amplitudes can be given as

$$\frac{\partial A_1(x,y,z;t)}{\partial t} = \mathrm{i}\,\Omega_{\rm p}^* A_2(x,y,z;t), \quad (8)$$

$$\frac{\partial A_2(x,y,z;t)}{\partial t} = (\mathrm{i}\Delta_{\rm p} - \gamma_2)A_2(x,y,z;t) + \mathrm{i}\,[G_{\rm s}^*(x,y,z) + \Omega_{\rm c}^*]A_3(x,y,z;t) + \mathrm{i}\,\Omega_{\rm p}A_1(x,y,z;t), \quad (9)$$

$$\frac{\partial A_3(x,y,z;t)}{\partial t} = (\mathrm{i}\Delta_{\rm s} - \gamma_3)A_3(x,y,z;t) + \mathrm{i}G_{\rm s}(x,y,z)A_2(x,y,z;t) + \mathrm{i}\,\Omega_{\rm c}A_2(x,y,z;t), \quad (10)$$

where $\gamma_i\,(i = 2, 3)$ is the decay rate of state $|i\rangle$, which is added phenomenologically.

Under the weak-field approximation, i.e. $\Omega_{\rm p} \ll \Omega_{\rm s}$, we can get $A_1(x, y, z; 0) \approx 1$ for all of the time t in the condition of considering the quasi-stationary-state solution of equations (9) and (10). Then, the probability amplitude $A_2(x, y, z;t)$ in the large time limit can be derived as

$$A_2(x,y,z) = \frac{D_2}{D}\Omega_{\rm p}, \quad (11)$$

where $D = |G_{\rm s}(x,y,z) + \Omega_{\rm c}|^2 - D_1D_2$, $D_1 = \Delta_{\rm p} + \mathrm{i}\gamma_2$ and $D_2 = \Delta_{\rm s} + \mathrm{i}\gamma_3$.

We define $n_{\rm e} = |A_2(x,y,z)|^2$ as the excited population. Thus, the excited population $n_{\rm e}$ can be explicitly expressed in the following form

$$n_{\rm e} = |A_2(x,y,z)|^2 = \frac{(\gamma_3^2 + \Delta_{\rm s}^2)|\Omega_{\rm p}|^2}{(|G_{\rm s}(x,y,z) + \Omega_{\rm c}|^2 + D_3)^2 + D_4^2}, \quad (12)$$

where $D_3 = \gamma_2\gamma_3 - \Delta_{\rm p}\Delta_{\rm s}$ and $D_4 = \gamma_3\Delta_{\rm p} + \gamma_2\Delta_{\rm s}$.

Equation (12) reflects the conditional position probability distribution of the atom in 3D space [34]. Therefore, the 3D atom localization behavior near point (x_0, y_0, z_0) (i.e. $x_0 = 2l\frac{\lambda}{4}, y_0 = 2m\frac{\lambda}{4}, z_0 = 2n\frac{\lambda}{4}$ with l as well as m and n being integers), including the increase of the detecting probability and improvement of the localization precision, can be controlled by adjusting the system parameters.

3. Numerical results and discussions

In this section, we investigate the conditional position probability distribution of the atom in 3D space via a few numerical calculations based on the excited population $n_{\rm e}$ in equation (12), and then achieve high-precision 3D atom localization by measuring the population of the levels $|2\rangle$. Here, a realistic candidate for the proposed atomic system can be found in ^{87}Rb atoms with the designated states chosen as follows [38]: $|^5S_{1/2}, F = 2\rangle$ as $|1\rangle$, $|^5P_{3/2}, F = 3\rangle$ as $|2\rangle$, $|^5D_{5/2}, F = 4\rangle$ as $|3\rangle$. To give a clear illustration, we select $\gamma_2 = \gamma_3 = 0.01\gamma$, $\Omega_{\rm s} = \gamma$, $\Omega_{\rm p} = 0.1\gamma$, and all the parameters used in the following numerical calculations are in the unit of γ. Subsequently, we present a few numerical results for 3D atom localization with different values of the relevant parameters to illustrate that high-precision 3D atom localization can be achieved in the present ladder-type three-level atomic system.

First of all, we investigate the influence of probe detuning $\Delta_{\rm p}$ on 3D atom localization near point (x_0, y_0, z_0) without considering the control field or the phase shifts of the standing-wave fields (i.e, $\Omega_{\rm c} = 0$, $\varphi = \phi = \eta = 0$). From figure 2,

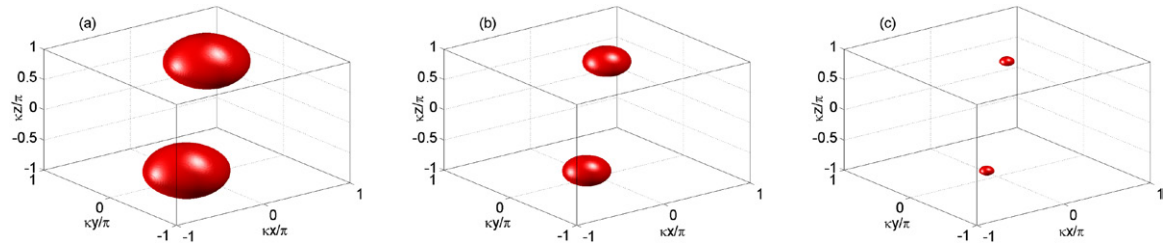

Figure 2. The excited population $n_e = 0.1$ as functions of $(\kappa x, \kappa y, \kappa z)$ for different probe detunings Δ_p. (a) $\Delta_p = 4.4\gamma$; (b) $\Delta_p = 6.4\gamma$; (c) $\Delta_p = 7.4\gamma$. Other values of the parameters are chosen as $\gamma_2 = \gamma_3 = 0.01\gamma$, $\Omega_s = \gamma$, $\Omega_p = 0.1\gamma$, $\Omega_c = 0$, $\Delta_s = 5\gamma$, $\kappa_1 = \kappa_3 = \kappa_5 = \kappa$, $\kappa_2 = \kappa_4 = \kappa_6 = \kappa$ and $\varphi = \phi = \eta = 0$.

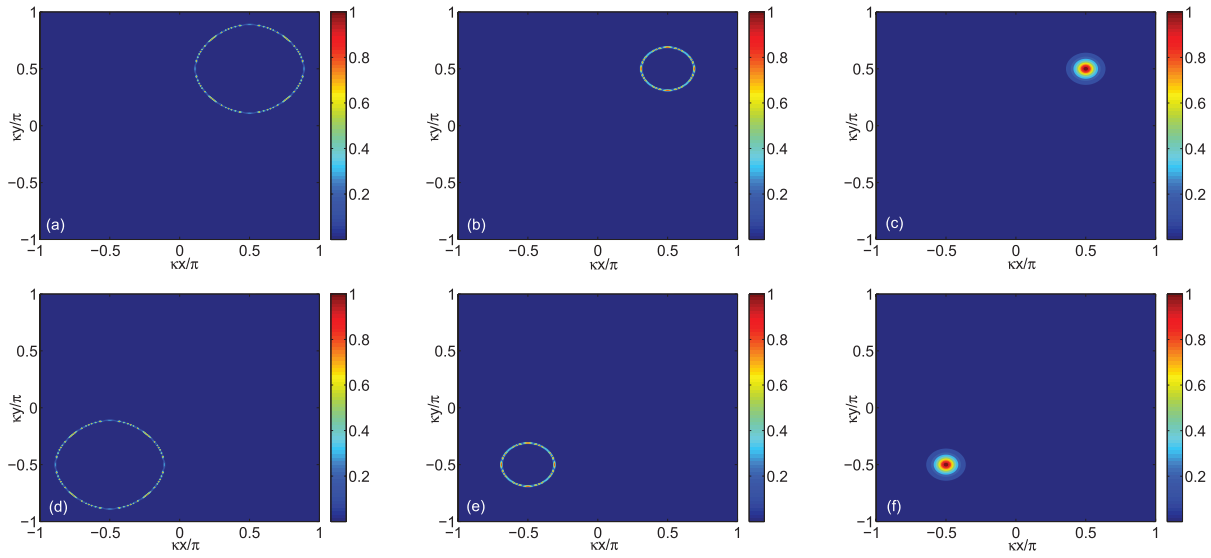

Figure 3. Density plot of the excited population n_e in the $x - y$ plane shown in figure 2. In the case of $\kappa z = \pi/2$, (a) $\Delta_p = 4.4\gamma$; (b) $\Delta_p = 6.4\gamma$; (c) $\Delta_p = 7.4\gamma$. In the case of $\kappa z = -\pi/2$, (d) $\Delta_p = 4.4\gamma$; (e) $\Delta_p = 6.4\gamma$; (f) $\Delta_p = 7.4\gamma$. Other values of the parameters are chosen as $\gamma_2 = \gamma_3 = 0.01\gamma$, $\Omega_s = \gamma$, $\Omega_p = 0.1\gamma$, $\Omega_c = 0$, $\Delta_s = 5\gamma$, $\kappa_1 = \kappa_3 = \kappa_5 = \kappa$, $\kappa_2 = \kappa_4 = \kappa_6 = \kappa$ and $\varphi = \phi = \eta = 0$.

one finds that the spatial distribution as well as the precision of 3D atom localization are dependent on probe detuning. To obtain a clearer picture about the conditional position probability distribution of the atom in the x–y plane, figure 3 shows the corresponding density plots of the excited population n_e in the plane. In the case of $\Delta_p = 4.4\gamma$ (see figures 2(a) and 3(a)–(d)), two ellipsoidal shells of the same size are situated in two subspaces $(-x, -y, -z)$ and (x, y, z), respectively. When probe detuning Δ_p increases to 6.4γ, keeping all other parameters fixed, although the localization patterns of atoms in two subspaces are still ellipsoid-like, the size of the two ellipsoidal shells becomes smaller (see figures 2(b) and 3(b)–(e)). More interestingly, when Δ_p is tuned from 6.4γ to 7.4γ, the size of the two ellipsoidal structures situated in subspaces $(-x, -y, -z)$ and (x, y, z) is further reduced, as shown in figures 2(c) and 3(c)–(f). A direct comparison in figures 2(a)–(c) implies that the precision of 3D atom localization in 3D space can be greatly improved when probe detuning Δ_p increases. Thus, high-precision and high-resolution 3D atom localization is indeed achieved by adjusting probe detuning.

In figure 4, we investigate the influence of the intensity of the control field Ω_c on 3D atom localization behavior in the absence of the phase shifts of the standing-wave fields (i.e. $\varphi = \phi = \eta = 0$). From figure 4, one finds that the atom can be completely localized in subspace $(-x, -y, -z)$, and the size of the ellipsoidal shell situated in subspace $(-x, -y, -z)$ becomes smaller with an increase in the intensity of the control field Ω_c from 9.5γ to 11.1γ. In such a case, it is worth pointing out that the precision of 3D atom localization can be significantly improved by adjusting the intensity of the control field to an appropriate value, and the maximum probability of finding the atom within a cubic optical wavelength is significantly improved by a factor of eight compared with [33, 34].

The interesting localization phenomena, as shown in figure 4, can be explained using the quantum interference effect in the dressed-state picture. By using the dressed-state picture, the bare-state levels $|2\rangle$ and $|3\rangle$ can be replaced by two dressed states $|-\rangle$ and $|+\rangle$ (see figure 1(b)), under the action of the control field Ω_c and the combination of three mutually perpendicular standing-wave fields $G_s(x, y, z)$. Such a subsystem is described by the interaction Hamiltonian operator $V_{int} = \Delta_s|3\rangle\langle 3| - [\Omega_c|3\rangle\langle 2| + G_s(x, y, z)|3\rangle\langle 2| + \text{H.c.}]$. Thus, the corresponding eigenequation [39] can be given by

$$\begin{bmatrix} -\lambda & -V_{32}^* \\ -V_{32} & \Delta_s - \lambda \end{bmatrix} \begin{bmatrix} c_2 \\ c_3 \end{bmatrix} = 0, \tag{13}$$

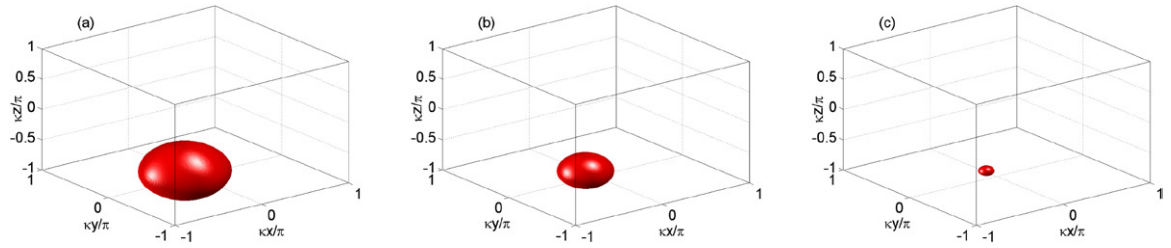

Figure 4. The excited population $n_e = 0.1$ as a function of $(\kappa x, \kappa y, \kappa z)$ for different intensities of the control field Ω_c. (a) $\Omega_c = 9.5\gamma$; (b) $\Omega_c = 10.5\gamma$; (c) $\Omega_c = 11.1\gamma$. Other values of the parameters are chosen as $\gamma_2 = \gamma_3 = 0.01\gamma$, $\Omega_s = \gamma$, $\Omega_p = 0.1\gamma$, $\Delta_p = 5\gamma$, $\Delta_s = 5\gamma$, $\kappa_1 = \kappa_3 = \kappa_5 = \kappa$, $\kappa_2 = \kappa_4 = \kappa_6 = \kappa$ and $\varphi = \phi = \eta = 0$.

where $V_{32} = G_s(x, y, z) + \Omega_c$ and $V_{32}^* = G_s^*(x, y, z) + \Omega_c^*$. $c_i (i = 2, 3)$ denotes the probability amplitude corresponding to the eigenstate $|i\rangle$. In order to ensure that equation (13) has a nontrivial solution, we have given the corresponding condition, i.e.

$$\begin{vmatrix} -\lambda & -G_s^*(x, y, z) - \Omega_c^* \\ -G_s(x, y, z) - \Omega_c & \Delta_s - \lambda \end{vmatrix} = 0. \tag{14}$$

By solving equation (14), the energy eigenvalues of the two dressed states can be obtained as

$$\lambda_\pm = \frac{\Delta_s \pm \sqrt{\Delta_s^2 + 4\,|G_s(x, y, z) + \Omega_c|^2}}{2}. \tag{15}$$

The corresponding energy eigenstates can be written as

$$\begin{aligned} |+\rangle &= \sin\theta|2\rangle + \cos\theta|3\rangle, \\ |-\rangle &= -\cos\theta|2\rangle + \sin\theta|3\rangle, \end{aligned} \tag{16}$$

together with

$$\begin{aligned} \sin\theta &= \frac{\lambda_+}{\sqrt{\lambda_+^2 + |G_s(x, y, z) + \Omega_c|^2}} \\ &= \frac{G_s(x, y, z) + \Omega_c}{\sqrt{\lambda_-^2 + |G_s(x, y, z) + \Omega_c|^2}}, \\ \cos\theta &= -\frac{\lambda_-}{\sqrt{\lambda_-^2 + |G_s(x, y, z) + \Omega_c|^2}} \\ &= \frac{G_s(x, y, z) + \Omega_c}{\sqrt{\lambda_+^2 + |G_s(x, y, z) + \Omega_c|^2}}. \end{aligned}$$

From equations (15) and (16), it is straightforward to show that when Δ_s is not equal to zero (i.e. $\Delta_s = 5\gamma$), the energy eigenvalues of the two dressed states obviously depend on $G_s(x, y, z)$ and the control field Ω_c, and two different transition channels (i.e. $|+\rangle \leftrightarrow |1\rangle$ and $|-\rangle \leftrightarrow |1\rangle$) will show up. When the intensity of control field Ω_c increases, a redistribution of the excited state population can obviously be observed (see figure 4). Physically, quantum interference induced by the control field Ω_c and the combination of three mutually perpendicular standing-wave fields $G_s(x, y, z)$ becomes a dominant mechanism, affecting the distribution of the excited population [36, 40, 41]. As a consequence, the atom is completely localized in subspace $(-x, -y, -z)$ with different atom localization precision, as shown in figure 4. In particular, for a larger intensity of control field (i.e, $\Omega_c = 11.1\gamma$, see figure 4(c)), we can obtain high-precision and high-resolution 3D atom localization within a narrow volume due to the presence of the quantum interference effect.

It is desirable to obtain the position of the atom when the atom passes through the standing-wave fields. The present scheme for 3D atom localization is based on the fact that the conditional probability distribution of the atoms carries the information about the atomic position. Therefore, one can extract the localization information by means of the similar measurement schemes for 1D and 2D atom localization reported in [14, 28]. We noticed that the previous scheme [28] for 2D atom localization had shown that the phase shifts played an important role in the spatial measurement of the atom in two-dimensions and a single atom localization peak could be observed when one chose slightly different wavelengths of the standing-wave fields. Here, we will investigate the influence of the phase shifts (φ, ϕ, η) of three orthogonal standing-wave fields on the behavior of 3D atom localization. In figure 5, we plot the excited population $n_e = 0.1$ as a function of $(\kappa x, \kappa y, \kappa z)$, dependent on the phase shifts (φ, ϕ, η) of three perpendicular standing-wave fields with slightly different wavelengths, without considering the control field Ω_c (i.e. $\Omega_c = 0$). In the condition of $\kappa_1 = \kappa_3 = \kappa_5 = \kappa$ and $\varphi = \phi = \eta = 0$, it can be found from figure 5(a) that two ellipsoidal shells of the same size are situated in two subspaces (x, y, z) and $(-x, -y, -z)$, respectively. Such a result is similar to the result of figure 2(b). When the phase shifts φ and ϕ are both equal to $2\pi/5$, and the wave vectors κ_1 and κ_3 are both equal to 0.85κ, the ellipsoidal shell in subspace $(-x, -y, -z)$ disappears, and the size of the ellipsoidal shell in subspace (x, y, z) becomes smaller, as shown in figure 5(b). Different from figure 5(a), the equal probability distribution of atoms is destroyed when the phase-shifts φ and ϕ of the corresponding standing-wave fields are nonzero, originating from the phase-dependent interference induced by the standing-wave fields. More interestingly, for the case in which $(\kappa_1, \kappa_3, \kappa_5) = (0.85\kappa, 0.85\kappa, 0.85\kappa)$ and $(\varphi, \phi, \eta) = (\frac{2\pi}{5}, \frac{2\pi}{5}, \frac{2\pi}{5})$, the structure of 3D localization with a small size in figure 5(c) still has an ellipsoid-like pattern, where the corresponding atom localization precision is further improved compared to figure 5(b). The above results can also be explained by the dressed states theory. When the intensity of the control field Ω_c is equal to zero, and the corresponding two-photon detuning Δ_s is equal to 5γ, the energy eigenvalues

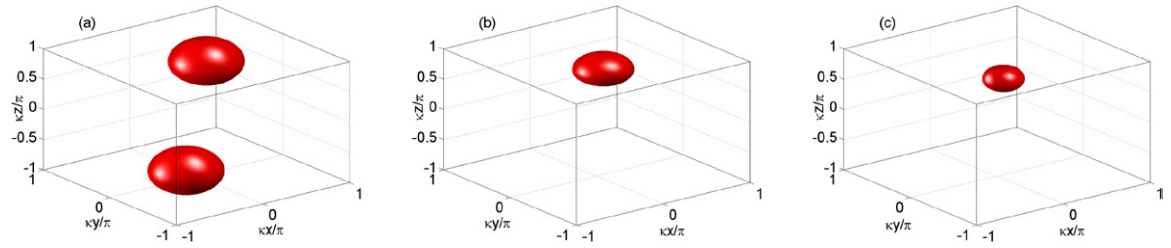

Figure 5. The excited population $n_e = 0.1$ as a function of $(\kappa x, \kappa y, \kappa z)$, dependent on the phase shifts (φ, ϕ, η) of the standing-wave fields with slightly different wavelengths. (a) $(\kappa_1, \kappa_3, \kappa_5) = (\kappa, \kappa, \kappa), (\varphi, \phi, \eta) = (0, 0, 0)$; (b) $(\kappa_1, \kappa_3, \kappa_5) = (0.85\kappa, 0.85\kappa, \kappa), (\varphi, \phi, \eta) = (2\pi/5, 2\pi/5, 0)$; (c) $(\kappa_1, \kappa_3, \kappa_5) = (0.85\kappa, 0.85\kappa, 0.85\kappa), (\varphi, \phi, \eta) = (2\pi/5, 2\pi/5, 2\pi/5)$. Other values of the parameters are chosen as $\gamma_2 = \gamma_3 = 0.01\gamma, \Omega_s = \gamma, \Omega_p = 0.1\gamma, \Omega_c = 0, \Delta_p = 5\gamma, \Delta_s = 5\gamma$ and $\kappa_2 = \kappa_4 = \kappa_6 = \kappa$.

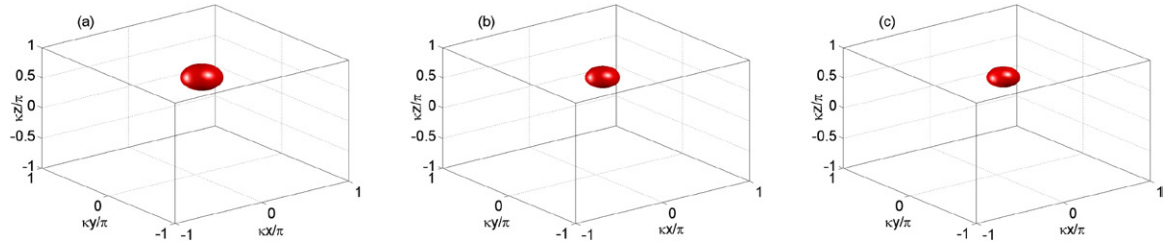

Figure 6. The 3D conditional position probability distribution as functions of $(\kappa x, \kappa y, \kappa z)$ for different values of the excited population n_e. (a) $n_e = 0.1$; (b) $n_e = 0.5$; (c) $n_e = 0.9$. Other values of the parameters are chosen as $\gamma_2 = \gamma_3 = 0.01\gamma, \Omega_s = \gamma, \Omega_p = 0.1\gamma, \Omega_c = 0, \Delta_p = 5\gamma, \Delta_s = 5\gamma, \kappa_1 = \kappa_3 = \kappa_5 = 0.85\kappa, \kappa_2 = \kappa_4 = \kappa_6 = \kappa$ and $\varphi = \phi = \eta = 2\pi/5$.

of the two dressed states obviously depends on $G_s(x, y, z)$. That is to say, the corresponding energy eigenvalues are varied with the phase shifts of three orthogonal standing-wave fields. In particular, when the phase-shifts φ with ϕ as well as η are equal to $2\pi/5$, and the wave vectors κ_1 with κ_3 as well as κ_5 are equal to 0.85κ (see figure 5(c)), the 3D localization space will become narrow, and the atom will be localized in volumes that are substantially smaller than a cubic optical wavelength. Thus, it is reasonable to obtain the single position information of the atom in 3D space by properly adjusting the phase-shifts in the condition of considering slightly different wavelengths of the standing-wave fields.

Last but not least, to obtain a better understanding of how the excited population n_e modifies 3D atom localization behavior, we draw plots of 3D conditional position probability distribution versus the normalized position $(\kappa x, \kappa y, \kappa z)$ for three different values of the excited population, as shown in figure 6. Figure 6 shows that the precision of 3D atom localization almost remains unchanged with an increase in the value of the excited population from $n_e = 0.1$ to $n_e = 0.9$. That is to say, in our present scheme, high-precision 3D atom localization can be achieved in a wide range of the excited state population distribution. The above results show the advantages of our present system not possessed by the previous schemes [33–36].

4. Conclusions

In conclusion, we have analyzed in detail the behavior of 3D atom localization in a ladder-type three-level atomic system, in which three orthogonal standing-wave fields align along the x, y and z directions, while the weak probe field and the control field propagate along the z direction. Due to spatial-position-dependent atom-field interaction, 3D atom localization can be achieved by the measurement of the excited population n_e. It is clearly shown that the precision of 3D atom localization is extremely sensitive to the detuning Δ_p of the probe field, the intensity of the control field Ω_c and the phase-shifts of the corresponding standing-wave fields with slightly different wavelengths. The main advantage of our proposed scheme is that we have obtained the single position information of the atom with high precision in 3D space, and the probability of finding the atom in 3D space is significantly improved by a factor of eight by adjusting the intensity of the control field Ω_c to $\Omega_c = 11.1\gamma$, originating from the quantum interference effect induced by the applied optical fields. Finally, it is worth noting that our proposed scheme for 3D atom localization may be useful for the high-precision measurement of the center-of-mass wave function of moving atoms and atom lithography.

Before ending, it should be noted that our present study focuses only on the cold atomic system, and the results of Doppler broadening effects can be included by first rewriting the corresponding detunings, i.e. $\Delta_p = \omega_p - \omega_{21} - \Delta_{a1}$ and $\Delta_s = \omega_p + \omega_s - \omega_{31} - \Delta_{a2}$, with $\Delta_{a1} \sim \kappa_p$ and $\Delta_{a2} \sim (\kappa_s + \kappa_p)$, the corresponding additional broadening effects, which can be suppressed in the cold atomic system.

Acknowledgments

This research is supported in part by the National Natural Science Foundation of China under grant nos. 11374050 and 61372102, by the Qing Lan project of Jiangsu, and by the Fundamental Research Funds for the Central Universities

under grant no. 2242012R30011, as well as by the Scientific Research Foundation of Graduate School of Southeast University no. YBJJ1522.

References

[1] Holland M, Marksteiner S, Marte P and Zoller P 1996 *Phys. Rev. Lett.* **76** 3683–6
[2] Kunze S, Dieckmann K and Rempe G 1997 *Phys. Rev. Lett.* **78** 2038–41
[3] Rudy P, Ejnisman R and Bigelow N P 1997 *Phys. Rev. Lett.* **78** 4906–9
[4] Quadt R, Collett M and Walls D F 1995 *Phys. Rev. Lett.* **74** 351–4
[5] Wu Y and Yang X X 2007 *Phys. Rev.* A **76** 013832
[6] Wu Y, Wen L L and Zhu Y F 2003 *Opt. Lett.* **28** 631–3
[7] Yang W X, Yang X X and Lee R K 2009 *Opt. Express* **17** 15402–8
[8] Yang W X, Chen A X, Lee R K and Wu Y 2011 *Phys. Rev.* A **84** 013835
[9] Liu S S, Liu S P, Zhu Z H and Yang W X 2016 *Laser Phys.* **26** 035401
[10] Qamar S, Zhu S Y and Zubairy M S 2000 *Phys. Rev.* A **61** 063806
[11] Kapale K T, Qamar S and Zubairy M S 2003 *Phys. Rev.* A **67** 023805
[12] Ghafoor F, Qamar S and Zubairy M S 2002 *Phys. Rev.* A **65** 043819
[13] Xu J and Hu X M 2007 *Phys. Lett.* A **366** 276–81
[14] Rahmatullah and Qamar S 2013 *Phys. Lett.* A **377** 1587–92
[15] Sahrai M, Tajalli H, Kapale K T and Zubairy M S 2005 *Phys. Rev.* A **72** 013820
[16] Kapale K T and Zubairy M S 2006 *Phys. Rev.* A **73** 023813
[17] Agarwal G S and Kapale K T 2006 *J. Phys. B: At. Mol. Opt. Phys.* **39** 3437
[18] Liu C, Gong S, Cheng D, Fan X and Xu Z 2006 *Phys. Rev.* A **73** 025801
[19] Evers J, Qamar S and Zubairy M S 2007 *Phys. Rev.* A **75** 053809
[20] Qamar S, Evers J and Zubairy M S 2009 *Phys. Rev.* A **79** 043814
[21] Asghar S and Qamar S 2013 *Opt. Commun.* **295** 145
[22] Ivanov V and Rozhdestvensky Y 2010 *Phys. Rev.* A **81** 033809
[23] Wan R G, Kou J, Jiang L, Jiang Y and Gao J Y 2011 *J. Opt. Soc. Am.* B **28** 10–7
[24] Wan R G, Kou J, Jiang L, Jiang Y and Gao J Y 2011 *J. Opt. Soc. Am.* B **28** 622–8
[25] Wan R G and Zhang T Y 2011 *Opt. Express* **19** 25823–32
[26] Wu J C and Ai B Q 2014 *Europhys. Lett.* **107** 14002
[27] Ding C L, Li J H, Yang X X, Zhang D and Xiong H 2011 *Phys. Rev.* A **84** 043840
[28] Rahmatullah and Qamar S 2013 *Phys. Rev.* A **88** 013846
[29] Zhu Z H, Yang W X, Chen A X, Liu S P and Lee R K 2015 *J. Opt. Soc. Am.* B **32** 1070–7
[30] Zhang D, Yu R, Li J H, Hao X Y and Yang X X 2014 *Opt. Commun.* **321** 138–44
[31] Wang Z P and Yu B L 2014 *Laser Phys. Lett.* **11** 035201
[32] Wang Z P and Yu B L 2014 *Laser Phys.* **24** 045203
[33] Qi Y H, Zhou F X, Huang T, Niu Y P and Gong S Q 2012 *J. Mod. Opt.* **59** 1092–9
[34] Ivanov V S, Rozhdestvensky Y V and Suominen K A 2014 *Phys. Rev.* A **90** 063802
[35] Hamedi H R and Mehmannavaz M R 2016 *J. Opt. Soc. Am.* B **33** 41–5
[36] Wang Z P and Yu B L 2015 *Quantum Inf. Process.* **14** 4067–76
[37] Meystre P and Sargent M III 1999 *Elements of Quantum Optics* (Berlin: Springer)
[38] Moon H S and Jeong T 2014 *Phys. Rev.* A **89** 033822
[39] Orszag M 2000 *Quantum Optics* (Berlin: Springer)
[40] Liu S P, Yang W X, Zhu Z H and Lee R K 2015 *Laser Phys. Lett.* **12** 095202
[41] Wu Y, Payne M G, Hagley E W and Deng L 2004 *Opt. Lett.* **29** 2294–6